

Classical Strongly Coupled QGP I : The Model and Molecular Dynamics Simulations

Boris A. Gelman, Edward V. Shuryak and Ismail Zahed

Department of Physics and Astronomy

State University of New York, Stony Brook, NY 11794-3800

We propose a model for the description of strongly interacting quarks and gluon quasiparticles at $T = (1 - 3)T_c$, as a classical and nonrelativistic colored Coulomb gas. The sign and strength of the inter-particle interactions are fixed by the scalar product of their classical *color vectors* subject to Wong's equations. The model displays a number of phases as the Coulomb coupling is increased ranging from a gas, to a liquid, to a crystal with antiferromagnetic-like color ordering. We analyze the model using Molecular Dynamics (MD) simulations and discuss the density-density correlator in real time. We extract pertinent decorrelation times, diffusion and viscosity constants for all phases. The classical results when extrapolated to the sQGP suggest that the phase is liquid-like, with a diffusion constant $D \approx 0.1/T$ and a bulk viscosity to entropy density ratio $\eta/s \approx 1/3$.

I. INTRODUCTION

The Quark-gluon plasma (QGP) is a high temperature phase of QCD. Here, the word *plasma* is used in the same sense as in electrodynamical plasma, that is a phase with free color charges that are screened [1] rather than confined by the medium. Lattice simulations have shown, that the QGP exists above the critical temperature $T > T_c \approx 170 \text{ MeV}$ of the QCD phase transition, in the deconfined and chirally symmetric phase.

Asymptotic freedom of Non-Abelian gauge theories, a property of QCD, insures that for high enough temperature $T \gg \Lambda_{QCD}$ this phase becomes *weakly* coupled (wQGP), with most of the particle interactions characterized by a small coupling $\alpha_s(p \approx T) \ll 1$. In this regime, the wQGP is a near-ideal gas of its fundamental constituents, quarks and gluons. Perturbative methods, such as hard thermal loops [2] and other resummations techniques, show how quarks and gluons are dressed and become quasiparticles with T -dependent dispersion curves and widths.

The QGP is experimentally studied using heavy ion collisions, such as dedicated experiments carried at the CERN SPS during the previous decade, and now at the BNL RHIC collider. RHIC can reach temperatures of about $2T_c$. The success of the hydrodynamical description for the observed collective flows at RHIC [3] has shown that all dissipative lengths are very short. The produced matter at RHIC *cannot* be a weakly coupled gas but a rather good liquid [4]. Recently, two of us [5] have suggested that the interaction of quasiparticles in the relevant temperature range at RHIC is strong enough to generate multiple marginal colored Coulomb bound states. Some of those states (charmonium) are observed in current lattice [6] simulations till about $2.5T_c$. The existence of these states, especially the colored ones, is still debated and warrant further numerical and independent checks on the lattice.

The effective potential energy of two static colored charges separated by a distance R , $U(R)$ can also be deduced from lattice simulations. Close to the crit-

ical temperature, the separation energy ΔU (the potential at infinity minus its value at some typical distance 0.3 fm) is $\Delta U \approx 4 - 1 \text{ GeV}$ in the temperature range $T = (1 - 1.2)T_c = 0.17 - 0.21 \text{ GeV}$. The ensuing Boltzmann penalty e^{-u} with $u = \Delta U/T \approx 20 - 5$ is mighty, indicating the dominance of potential over kinetic energy. This regime is now called a *strongly* coupled QGP (sQGP). Its structure and consequently its *transport properties* are radically different from a wQGP to which it is expected to fold at very high temperature.

In the traditional context of an electromagnetic plasma, the term “strongly coupled” plasma has a similar meaning. Ionic or dusty plasmas have charged ions with large masses, and thus are essentially classical. The standard dimensionless parameter characterizing the strength of the interparticle interaction in a classical plasma is Γ the ratio of potential to kinetic energy

$$\Gamma = \frac{(Ze)^2}{a_{WS}T} \quad (1)$$

where Ze, a_{WS}, T are respectively the ion charge, the Wigner-Seitz radius $a_{WS} = (3/4\pi n)^{1/3}$ and the temperature *. Γ is convenient to use because it only involves the *input* parameters, such as the temperature and density. However, one should keep in mind that the real interaction parameter is the *output* dimensional parameter u ,

$$u = \frac{U}{T} \quad (2)$$

where $U = \langle V \rangle$ is the average interaction of a particle with all its neighbors. This is the ratio that enters the effective Boltzmann exponent, and defines all correlation functions.

Since u is proportional to Γ , one usually defines the weakly coupled regime for $\Gamma \ll 1$ and the strongly coupled regime in the opposite limit $\Gamma \gg 1$. Extensive stud-

*We do not use k_B and thus measure temperature in energy units.

ies of the one-component plasma (OCP) in electrodynamics, using both MD and analytical methods over the past decades, have revealed the following regimes: **i.** a gas regime for $\Gamma < 1$; **ii.** a liquid regime for $\Gamma \approx 10$; **iii.** a glass regime for $\Gamma \approx 100$; **iv.** a solid regime for $\Gamma > 300$. For a review see e.g. [8].

Another physical system closer to what we will discuss in this work is a classical two-component plasma (TCP) with both positive and negative charges. Examples are molten or frozen salts with ions of comparable masses, as in the sQGP. Hydrogen plasmas are better studied, but the underlying charges carry very different masses, so the ensuing results bear no insight to the sQGP where the masses are likely comparable.

Quantum effects will be schematically incorporated in the form of a *localization energy*, providing a repulsive core for the 2-particle interaction irrespective of the charge. In the future we plan to study more quantum corrections to classical MD, in particular the role of the exclusion principle, and the relation between classically *correlated charges* and quantum bound states.

We are certainly aware of many cases of quantum plasmas. An quantum electron plasma in metals is quantum and thoroughly studied, but repulsive nature of the electron-electron interaction excludes the formation of bound states and is very different from QGP we are interested in. Only weak induced electron-electron interaction leads Cooper pairing in superconductors. Excitons in semiconductors, in a plasma of particles and holes, are even closer to our problem. Recent progress in trapped strongly coupled fermionic atoms have further elucidated how the transition to Bose-condensed pairs takes place. However, in all these cases one needs novel tools to study quantum effects dynamically: the existing ones, such as e.g. restricted paths Monte Carlo, use Euclidean time correlators which (like those from lattice QCD) are good for thermodynamical observables but next-to-impossible to use for transport properties. The MD approach, whatever crude it can be, is an invaluable classical tool which directly provides real-time correlators. Furthermore, pertinent quantum corrections can be added later, as it is done in some atomic systems.

The model we propose in this work combines features of strongly coupled Abelian TCP, with non-Abelian features proper to QCD in the form of classical color vectors for the underlying charges. The main interparticle interaction is proportional to the dot-product of the color vectors, which of course can be attractive, repulsive or even null if the color vectors of the particles are orthogonal to each other. Dynamics of color vectors as well as particle coordinates are described by classical equations of motion (EoM), and thus can be studied by MD simulations, which are less involved than the corresponding coupled hierarchy of quantum Green's functions. Below, we will argue for which values of the parameters this model can be useful for understanding the sQGP. Before we will do so, the model will be defined and studied in its own right.

II. CLASSICAL QUARK-GLUON PLASMA, CQGP

A. The model

The model is based on the following main assumptions:

- i.** The particles are heavy enough to move nonrelativistically, with masses $M \gg T$;
- ii.** The inter-particle interaction is dominated by colored electric (Coulomb) interactions, with all magnetic effects (like e.g. spin forces) ignored;
- iii.** The color representations are large, so that color operators t^a can be represented by their average, classical color vectors.

The parameters of the model include the particle mass M and their density n . The main interaction potential is proportional to the dot-product of the unit color vectors times the standard Coulomb interaction strength. The notations we use parallel the conventions in EM plasmas and in QCD. The relation between the two is defined as

$$(Z_\alpha e)^2 = C_\alpha \frac{g^2}{4\pi} \quad (3)$$

where Z_α^2 in EM is C_α in QCD, the Casimir operator eigenvalue for \bar{q}, q, g , while $e^2 = g^2/4\pi$ [†]. When needed, we will “input” the Debye screening mass” M_D , if the classical screening of plasma charges derived dynamically from MD would not be an accurate representation of the effective forces between quasiparticles in the sQGP.

In QCD, all the effective parameters used here are functions of the temperature T and the baryon chemical potential μ , or of a point at the QCD phase diagram. In a heavy ion collision, those are defined by the collision energy and centrality of the collision. Furthermore, for each volume element the cooling of the matter during its expansion is well approximated by the adiabatic (fixed entropy/baryon densities) path on the phase diagram, related T and μ .

As a first approximation, baryonic charge play little role at RHIC and thus one can set $\mu = 0$ and think of only one parameter, the temperature T , defining matter properties. Therefore, when we attempt to map the MD results for the cQGP into sQGP, all the parameters of the model mentioned above should be converted to temperature, as we will detail. In way, the classical model we are about to discuss in an unrestricted n-dimensional parameter space, will be useful for the sQGP through a 1-dimensional slicing of the n-dimensional space. Probing the n-dimensional parameter space for the model is useful theoretically. Much like EM plasmas, the dimensionless parameter (1) will be key in characterizing the

[†]Note that the standard notations used in EM and QCD differ by 4π in the Lagrangian and all subsequent formulae.

transition from a weakly coupled regime with $\Gamma \ll 1$, to a strongly coupled regime $\Gamma \gg 1$.

At very low temperatures T or very large Γ , any classical system will freeze. Therefore, the low temperature behavior is dominated by the lowest ordered state. Here, we recall that in general, the Abelian 2-component plasma freezes to an ionic crystal much like ordinary salt $NaCl$. The non-Abelian plasma under consideration freezes also to *cubic crystal* with *ferromagnetic* (alternating) order of the classical color vectors. A direction in classical color space is selected randomly, through spontaneous symmetry breaking of the global color group, with alternating directions of the color vectors along the crystal axes.

B. The equations of motion

The specific model Hamiltonian is

$$H = \sum_{\alpha i} \frac{p_{\alpha i}^2}{2m_{\alpha}} + V_C + V_{\text{core}} \quad (4)$$

with the standard kinetic energy, the colored Coulomb interaction V_C and the repulsive core V_{core} respectively. The colored Coulomb part is

$$V_C = \sum_{\alpha i \neq \beta j} \frac{Q_{\alpha i}^a Q_{\beta j}^a}{|\vec{x}_{\alpha i} - \vec{x}_{\beta j}|} \quad (5)$$

The sums are over the species $\alpha = q, \bar{q}, g$ and their respective numbers N_{α} . We will specify V_{core} below.

Thus our phase space coordinates are the position (x_{α}), momentum (p_{α}) and color (Q_{α}). The latter rotates under a gauge transformation

$$Q^a \rightarrow D^{ab}(\Lambda) Q^b \quad (6)$$

showing that (5) is gauge invariant. Only the Coulomb-like interaction was retained in (5) since the magnetically induced interactions are subleading non-relativistically. This is the case for all spin and local many-body forces. for instance the local 3-body gluon-induced interaction

$$\sum_{\alpha i \neq \beta j \neq \gamma k} Q_{\alpha i}^a Q_{\beta j}^b Q_{\gamma k}^c (f^{abc} \mathbf{F} + d^{abc} \mathbf{D}) \quad (7)$$

is subleading $\mathbf{F} \approx \mathbf{D} \approx \nabla/m$. Non-local many-body interactions as induced by the 2-body Coulomb and core interactions are important and will be resummed to all orders using MD.

The EoM for the phase space coordinates follow from the usual Poisson brackets. For the standard coordinates they are

$$\{x_{\alpha i}^m, p_{\beta j}^n\} = \delta^{mn} \delta_{\alpha\beta} \delta_{ij} \quad (8)$$

For the color coordinates they are

$$\{Q_{\alpha i}^a, Q_{\beta j}^b\} = f^{abc} Q_{\alpha i}^c \quad (9)$$

the classical analogue of the $SU(N_c)$ color commutators, with f^{abc} the known structure constants of the color group. The classical color vectors are all adjoint vectors with $a = 1 \dots (N_c^2 - 1)$. For simplicity only the non-Abelian group $SU(2)$ will be considered, with 3d color vectors. The difference between quarks and gluons follow from their respective Casimir assignments.

Although the brackets (9) do not look like the usual canonical relations between coordinates and momenta, they actually are. Indeed, a more standard phase space description requires the use of the Darboux parameterization [9]

$$Q = (\Phi^A, \Pi^A) \quad (10)$$

with $A = 1, \dots, N_c(N_c - 1)/2$ now satisfying standard canonical commutation relations

$$\{\Phi^A, \Pi^B\} = \delta^{AB} \quad (11)$$

the Φ 's are angular coordinates and the Π 's are angular momenta. The Π 's are identified with the fixed Casimirs of $SU(N_c)$ which are conserved by the equations of motion. For example, for $N_c = 2$, the 3 components of the color vector conserve one Casimir operator C_2 (the color vector's length). Without loss of generality, the Darboux coordinates may be chosen as

$$(Q_1 \pm iQ_2, Q_3) = (\sqrt{J^2 - \Pi^2} e^{\pm i\Phi}, \Pi) \quad (12)$$

with $J^2/3 = C_2$. For $N_c = 3$ there the color vector is 8-dimensional, with 2 fixed Casimirs ($Q^a Q^a$) and ($d^{abc} Q^a Q^b Q^c$), and 6 variables. In this case, the Darboux set is more involved, but can be parametrized with 3 angles and 3 conjugate momenta. We will not be working with Darboux-based EoM below.

The pertinent equations of motion for our classical Coulomb gas resulting from (4) and the Poisson brackets are

$$\begin{aligned} \dot{x}_{\alpha i}^n &= \{H, x_{\alpha i}^n\} = \frac{p_{\alpha i}^n}{m_{\alpha}} \\ \dot{p}_{\alpha i}^n &= \{H, p_{\alpha i}^n\} = g E_{\alpha i}^{an} Q_{\alpha i}^a \\ \dot{Q}_{\alpha i}^a &= \{H, Q_{\alpha i}^a\} = g f^{abc} Q_{\alpha i}^b A_{\alpha i 0}^c \end{aligned} \quad (13)$$

with

$$\begin{aligned} \vec{E}_{\alpha i}^a &= -\vec{\nabla}_{\alpha i} A_{\alpha i 0}^a \\ &= -\vec{\nabla}_{\alpha i} \sum_{\beta j \neq \alpha i} \frac{g Q_{\beta j}^a}{|\vec{x}_{\alpha i} - \vec{x}_{\beta j}|} \end{aligned} \quad (14)$$

The last of the three equation of motion in (13) is also known as Wong's equation [10]. Due to the antisymmetric nature of the structure constant f^{abc} , it has the form of rotation of the color vector conserving its length (classical precession). For $SU(2)$ this is the only Casimir, while for higher color representations more Casimirs are involved. We expect the resulting EoM to generate a ballet of classical precession conserving all these Casimirs.

III. NUMERICAL STUDIES USING MOLECULAR DYNAMICS

In this paper we will outline the basic ingredients involved in the MD analysis of (13). We first discuss what the pertinent scales are and how they are set. Second, we briefly comment on the numerical analysis used to deal with long-range Coulomb forces.

A. Potential and units

The MD simulation is basically a numerical solution of EoM starting from some initial conditions. The method was developed in the early days of computers in the 1950's, and applied extensively for the studies of simple liquids and plasmas. It is the most straightforward way to access transport properties such as the diffusion coefficient D , the bulk viscosity η , the heat conductivity λ , as well as pertinent decorrelation functions and times.

In standard 2-component plasma physics MD simulations, the interparticle potential is chosen as

$$V(r) = V_{\text{core}} + V_C = \left(\frac{e^2}{\lambda}\right) \left[\frac{1}{n} \left(\frac{\lambda}{r}\right)^n + \frac{Q_i Q_j}{r}\right] \quad (15)$$

with $r = |\vec{x}_i - \vec{x}_j|$ and $Q_i, Q_j = \pm 1$ are respective charges. The repulsive core potential V_{core} ensures overall matter stability with n some large parametric number. For atomic systems $n = 9$. For molten salts the core follows from the intrinsic repulsion of the atomic electrons.

Since this is the first paper in a series on this model, and as we are mostly interested in understanding the role played by the non-Abelian color variables, we have carried the numerical MD analysis for both the Abelian and non-Abelian charges. Both analysis were carried in parallel to understand the differences between discrete \pm charged plasmas and our classically colored SU(2) plasma with Q^a charges. Therefore, the same V_{core} was kept in the non-Abelian simulation.

The microscopic motivation in QCD for V_{core} stems from the short range part of the inter-particle interactions. Needless to say that this is a hard question, and not much is known about it from first principles whether in the intermediate coupling region ($\alpha_s \approx 1/2$) or the very strong coupling region ($\alpha_s \approx 1$ or $\Gamma \gg 1$).

One reason for an effective repulsion at short distance is the so called quantum localization potential

$$V_{\text{loc}} \approx \frac{\hbar^2}{mr^2}. \quad (16)$$

Such potentials are usually used in classical studies/simulations of light atoms, e.g. solid He. Note that this term has a lower power $n = 2$ rather than $n = 9$ used in V_{core} . This not a much importance as any $n > 1$ stabilizes the Coulomb attraction at short distances. The net effect of

the quantum localization is the introduction of a dimensional parameter, i.e. \hbar in natural classical units.

i. Length unit : At any n , the minimum of the potential is at $r = \lambda$. So λ sets the basic length scale, and from now on all distances are measured in units of λ . For example, a close cubic-packing density with $n_{cp} = 1/\lambda^3$ will be written as $n_{cp} = 1$. **ii. Time unit :** The unit of time τ_0 will be set by the natural frequency of a screened Coulomb system, its plasma frequency

$$\tau_0 = \omega_p^{-1} = \left(\frac{m}{4\pi n e^2}\right)^{1/2} \quad (17)$$

iii. Mass unit : This is naturally given by the particle mass m . Thus all important time correlators have a characteristic length of order 1 in τ_0 . In contrast, all MD runs are typically few hundreds or thousands τ_0 to insure statistical equilibrium.

This fixes the three basic units used in our analysis. For instance, the kinetic energy is measured in obvious units of $m\lambda^2/\tau_0^2$. The strength of the Coulomb potential, if measured in such units, is

$$\left(\frac{e^2}{\lambda}\right)/\left(\frac{m\lambda^2}{\tau_0^2}\right) = \frac{1}{4\pi} \frac{1}{n\lambda^3} \quad (18)$$

so that it is defined directly by the particle density. The temperature, in the same units, can be defined via averaged (dimensionless) velocities as $(3/2)T = \langle v^2/2 \rangle$. Finally the main parameter u in (2) can be obtained from simulation, as the ratio of the *measured* total mean potential to the total kinetic energy.

B. Technical details

There are readily available numerical packages for solving the set coupled set of differential equations of the type (13). In our case, their accuracy is tested through energy conservation and color vectors remaining on the unit sphere. We have used the package from the CERN Library in double precision and tested its accuracy for both energy and color conservation.

The many particle problem in a box requires the introduction of boundary conditions. We chose periodic boundary conditions. When a particle crosses one side, it reappears on the opposite side. We can visualize space as filled with many mirror cubes, piled next to each other. When one particle crosses out of the central cube, its mirror image enters from the opposite cube. The inter-particle potential in this many-cube world is periodic under cubic translation by \vec{L} , i.e.

$$V_{ij} = \sum_{n_x, n_y, n_z = -\infty}^{+\infty} V(\vec{x}_i - \vec{x}_j + n\vec{L}) \quad (19)$$

So as a particle crosses the boundary, there is no change in the force or the potential since (19) is truly periodic.

In practice, the sum in (19) is only carried over few adjacent cubes or mirror images, causing an overall loss of periodicity. As a result, the forces at the faces of the cube jump slightly thereby causing random kicks on the crossing particles. This gradually heats the system and should be controlled. The more long range the potential is, the more severe the heating.

Traditionally the Bethe polynomials for Ewald sums are used to overcome this heating phenomenon caused by the truncation. We have found this procedure not sufficiently accurate for the amount of complexity it introduces. Indeed, it leads to a factor of 50 suppression of the electric field normal to the cubic interface. Current computers easily allow for keeping up to 3-4 mirror images on each side of a central cube, thereby reducing the net electric field by orders of magnitude.

Another practical way to deal with this problem is introduction of a very small friction into the EoM, which can compensate the heating effect caused by the random forces at the cubic interface. Our typical runs consists of $4^4 = 64$ or $6^4 = 1296$ particles all of the same species.

C. Structure factor

The static and dynamic properties of a liquid are determined by various correlations functions. One of the most useful of these functions is a density-density correlation function or structure factor defined as,

$$G(r, t) = \frac{1}{n} \left\langle \rho(\vec{x}, t) \rho(\vec{0}, 0) \right\rangle, \quad (20)$$

with $r = |\vec{x}|$ and $\rho(\vec{x}, t)$ being the particle density at the position \vec{x} at time t ,

$$\rho(\vec{r}, t) = \sum_{i=1}^N \delta(\vec{x} - \vec{x}_i(t)), \quad (21)$$

Here, $n = N/V$ is the particle density and the averaging in (22) is carried over an equilibrium ensemble [‡].

Assuming translational invariance and isotropy, the classical density-density correlation function can be written as,

$$G(r, t) = \frac{1}{N} \left\langle \sum_{i=1}^N \sum_{j=1}^N \delta(\vec{x} + \vec{x}_i(0) - \vec{x}_j(t)) \right\rangle, \quad (22)$$

with N is the number of particles, $\vec{x}_i(t)$ is the position of the i th-particle at time t . $G(r, t)$ characterizes the likelihood to find 2 particles a distance r away from each other at time t .

[‡]In a given MD simulation the total energy and number of particles of a system is kept constant. This corresponds to using a microcanonical ensemble.

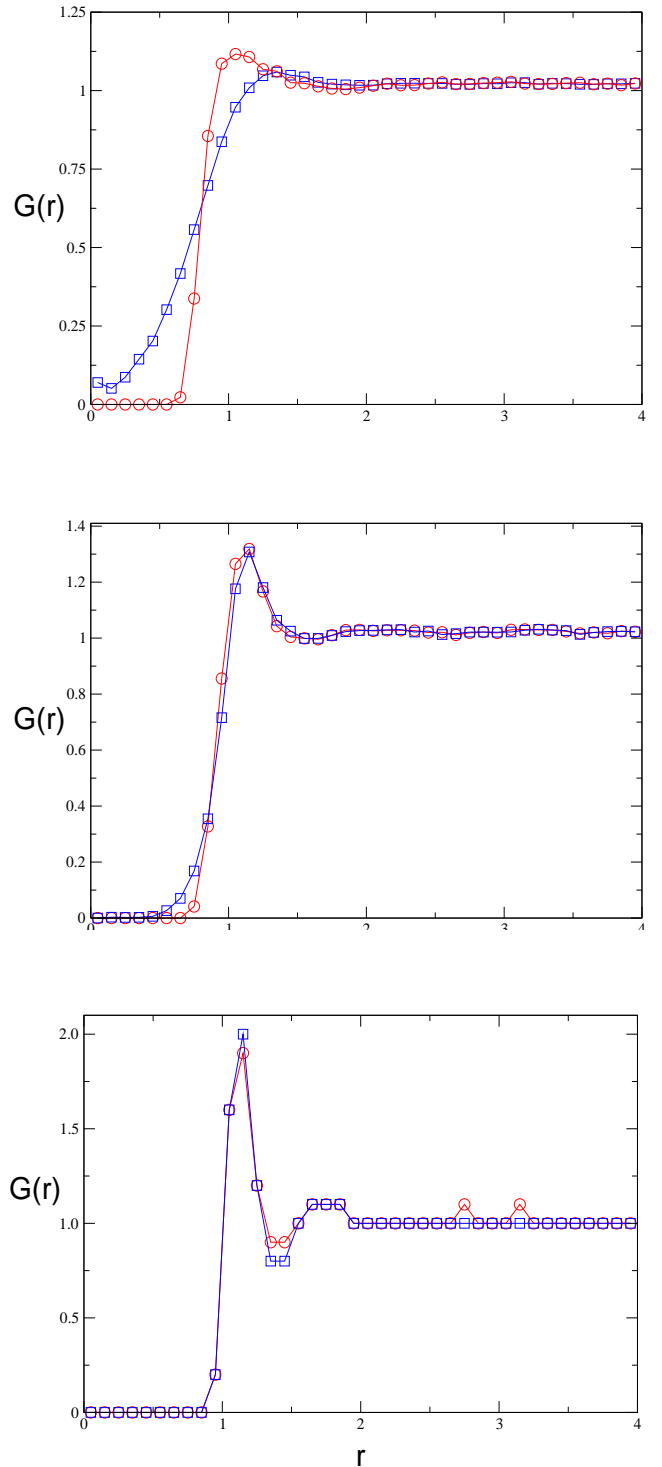


FIG. 1. G_d correlation function for $\Gamma = 0.83, 31.3, 131$, respectively. Red circles correspond to $t^* = 0$, and blue squares correspond to $t^* = 6$.

The density-density correlation function (22) can be written as a sum of two parts referred to as the van Hove or *self-correlation* G_s , and the *distinct-correlation* G_d ,

$$G(\vec{x}, t) = G_s(\vec{x}, t) + G_d(\vec{x}, t), \quad (23)$$

where

$$G_s(\vec{x}, t) = \frac{1}{N} \left\langle \sum_{i=1}^N \delta(\vec{x} + \vec{x}_i(0) - \vec{x}_i(t)) \right\rangle, \quad (24)$$

and,

$$G_d(\vec{x}, t) = \frac{1}{N} \left\langle \sum_{i \neq j}^N \delta(\vec{x} + \vec{x}_i(0) - \vec{x}_j(t)) \right\rangle. \quad (25)$$

We have measured a large selection of such function, as a typical examples let us present here G_d at three values of the coupling, moderate, strong and very strong, $\Gamma = 0.83, 31.3, 131$, see Fig.1. One sees from those that in the first case a relatively weak correlation between the particles, at distance 1 corresponding to the potential minimum, which relaxes rather quickly with time. The correlation is more robust in the second “liquid” case, and is very stable and is accompanied by extra peaks in a “solid” last case.

D. Transport coefficients

An important aspect of the strongly coupled plasmas is their dramatic change in transport properties in comparison to weakly coupled plasmas. The current MD simulations can be used to study the bulk transport properties at strong coupling. In particular, the shear and bulk viscosities, diffusion constant, thermal conductivity, color conductivity etc. A simple way to obtain these transport coefficients is via Green-Kubo relations. These relations give the transport coefficients in terms of the integrals of the equilibrium time-dependent correlation functions.

In the case of the self-diffusion the corresponding correlation function is the velocity autocorrelation function,

$$D(\tau) = \frac{1}{3N} \left\langle \sum_{i=1}^N \vec{v}_i(\tau) \cdot \vec{v}_i(0) \right\rangle, \quad (26)$$

where $\vec{v}_i(\tau)$ is the velocity of a particle i at time τ . The velocity autocorrelation functions are shown in Fig. 2 for $\Gamma = 0.83, 31.3, 131$ respectively. This refers to the non-ideal gas, liquid and crystal of the (one species) cQGP.

The diffusion constant is the integral of the velocity autocorrelation function,

$$D = \int_0^\infty D(\tau) d\tau. \quad (27)$$

Fig. (3) shows a log-log plot of the diffusion constant as a function of Γ . The dependence of D on Γ is linear and can be approximately described by a simple power

$$D \approx \frac{0.4}{\Gamma^{4/5}} \quad (28)$$

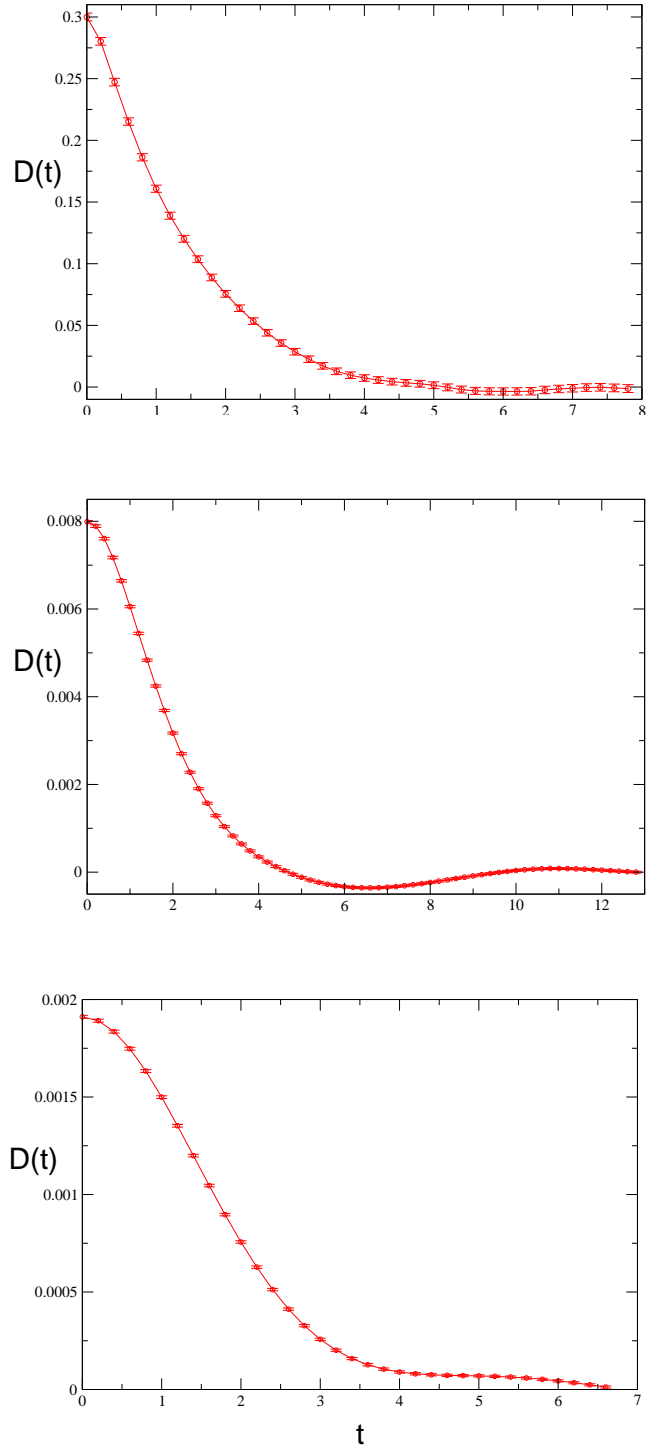


FIG. 2. Velocity autocorrelation function $D(\tau)$ for $\Gamma = 0.83, 31.3, 131$.

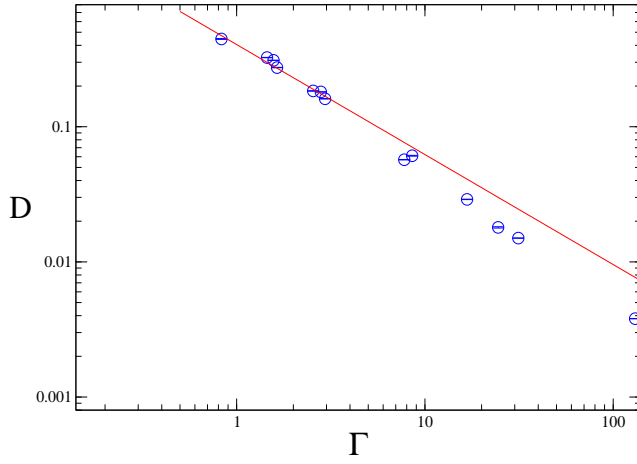


FIG. 3. The diffusion constant of a one species cQGP as a function of the dimensionless coupling Γ . Blue points are the MD simulations; the red curve is the expression (28).

The viscosity coefficients are given in terms of time autocorrelation function of the stress-energy tensor,

$$\eta(\tau) = \frac{1}{3TV} \left\langle \sum_{x < y} \sigma_{xy}(\tau) \sigma_{xy}(0) \right\rangle, \quad (29)$$

where $\sum_{x < y}$ denotes a sum over the three pairs of distinct tensor components (xy, yz and zx). The off-diagonal parts stress-energy tensor are given by

$$\sigma_{xy} = \sum_{i=1}^N m_i v_{ix} v_{iy} + \frac{1}{2} \sum_{i \neq j} r_{ij,x} F_{ij,y}, \quad (30)$$

and cyclically, with $\vec{r}_{ij} = \vec{x}_j - \vec{x}_i$ and \vec{F}_{ij} is the force on particle i due to particle j . The stress-tensor correlation functions are shown in Fig. 4 for $\Gamma = 0.83, 31.3, 131$ respectively.

The Green-Kubo relation for the the coefficient of the shear viscosity is,

$$\eta = \int_0^\infty \eta(\tau) d\tau. \quad (31)$$

The coefficient of shear viscosity as a function of Γ is shown in fig. 5. For small Γ the viscosity is large since the mean-free path is large in a gas-like phase. The viscosity is minimum in the liquid phase, and rises slowly in the crystal phase at large Γ . The coefficient η is approximately fitted by

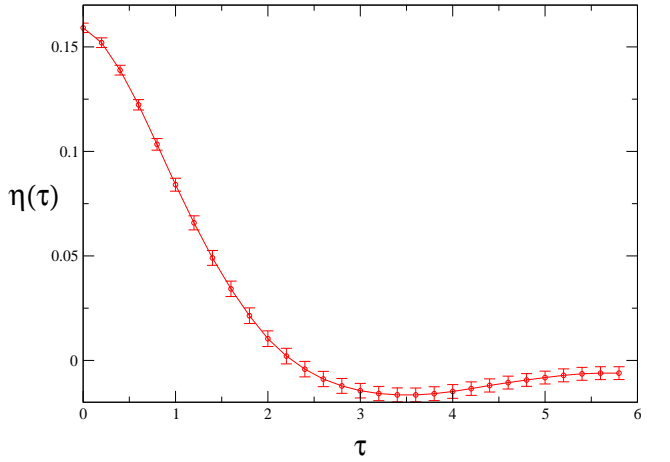
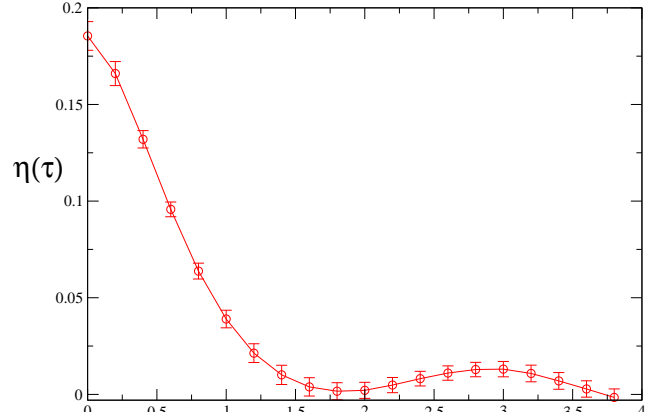
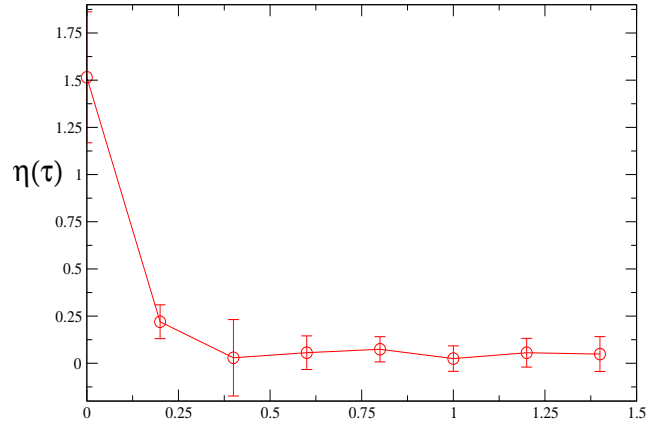


FIG. 4. Stress-tensor autocorrelation function $\eta(\tau)$ for $\Gamma = 0.83, 31.3, 131$.

$$\eta \approx 0.001 \Gamma + \frac{0.242}{\Gamma^{0.3}} + \frac{0.072}{\Gamma^2}. \quad (32)$$

Notice that the fit misses $\eta \approx 0.1$ at $\Gamma = 10$ which is the lowest viscosity measured in the current cQGP.

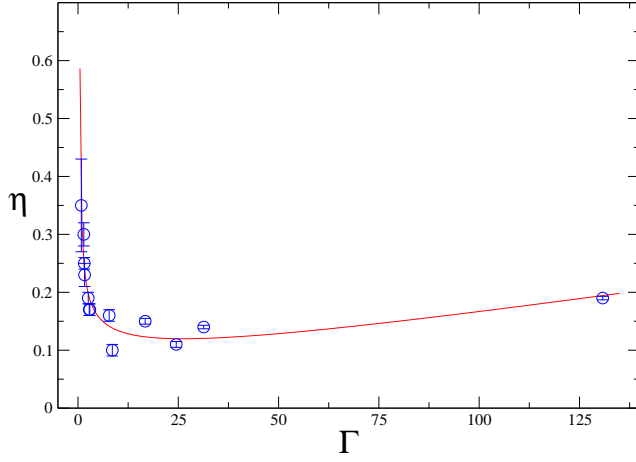


FIG. 5. Shear viscosity of one species cQGP as a function of the dimensionless coupling Γ . Blue points are the MD simulations; the red curve is the fit in eq. (32).

The stress-tensor auto-correlation function can be used to determine the viscous decorrelation time τ_η , defined as

$$\tau_\eta = \frac{\eta}{\eta(0)}, \quad (33)$$

where $\eta(0)$ is the value of the stress-energy auto-correlation function at time $t = 0$. The values of $\eta(0)$ and τ_η as a function of Γ are shown in Fig. 6 and Fig. 7, respectively.

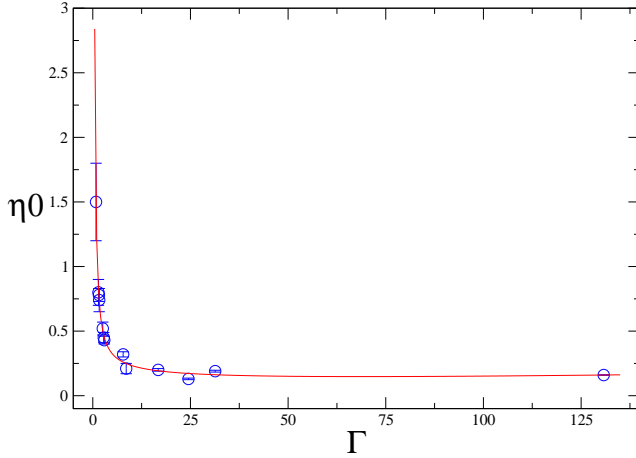


FIG. 6. Values of stress-energy auto-correlation at zero time of a one species cQGP as a function of the dimensionless coupling Γ . The blue points are the MD simulations; the red curve is the fit in eq. (34).

The functional dependence on Γ of $\eta(0)$ is

$$\eta(0) \approx 0.0005 \Gamma + \frac{0.77}{\Gamma^{1.57}} + \frac{0.44}{\Gamma^{0.33}}. \quad (34)$$

while that of the decorrelation time is

$$\tau_\eta \approx 0.239 + 0.091 \sqrt{\Gamma}. \quad (35)$$

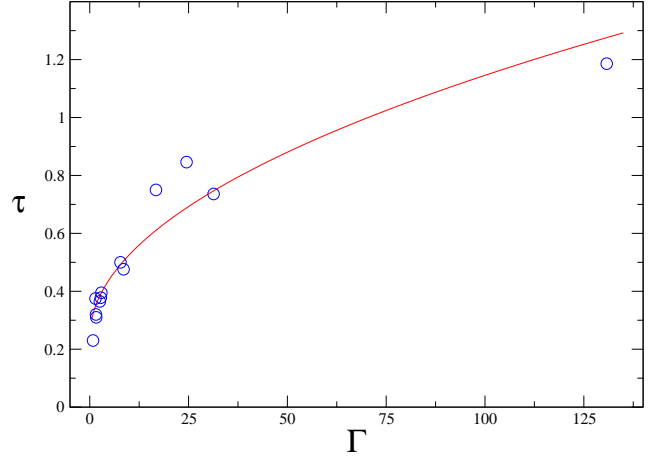


FIG. 7. The viscous decorrelation time for the stress-energy tensor time correlator as a function of the dimensionless coupling Γ . The blue points are the MD simulations; the red curve is the fit in eq. (35).

E. Potential energy

Another useful observable that can be determined from MD simulations is the total potential energy U normalized to T . This ratio as a function of Γ is shown in Fig. 8. The parametric dependence of this ratio on Γ is given by,

$$\frac{U}{NT} \approx -4.9 - 2\Gamma + 3.2\Gamma^{1/4} + \frac{2.2}{\Gamma^{1/4}}. \quad (36)$$

At large Γ the crystal phases sets in, and the potential energy asymptotes $U/NT \approx -2\Gamma$ which is a measure of the Madelung constant. A full theoretical analysis of (36) will be given in the sequel II.

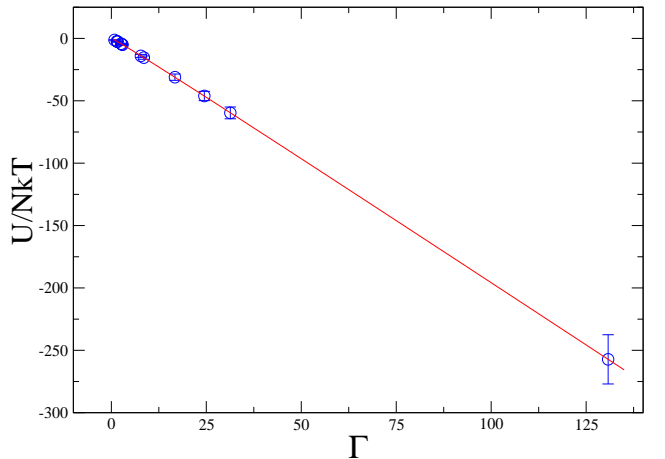


FIG. 8. Ratio of the potential energy to NT of a one species cQGP as a function of the dimensionless coupling Γ . The blue points are the MD simulations; the red curve is the fit in eq. (36).

IV. COMPARISON WITH SQGP

A qualitative mapping of the one species cQGP described above into sQGP can be made with the by adjusting the three basic scales described above, namely that of the length, the time and the mass. As we have repeatedly indicated above, all parameters of the model are functions of the temperature T in the sQGP. In this section we provide heuristic arguments for what the parameters are using a simple description of the sQGP at $T = 1.5 - 3 T_c$. (It is used as a reference point because more lattice data are available for it than for T close to T_c .)

As discussed above, the unit of length is λ the minimum of the potential. Since the repulsive part mocks up the quantum repulsion at short distances, the effective inter-particle potential is [§]

$$V_{\text{eff}} = \frac{\hbar^2}{2mr^2} - \frac{C\alpha_s}{r} \quad (37)$$

with a minimum at $r_0 = \hbar^2/(mC\alpha_s) = \lambda$. C is the pertinent Casimir for quarks and gluons.

The quasiparticle mass, defined as its energy at zero momentum, is at $T = (1.5-3)T_c$ about constant $m \approx 5T_c$ both for quark and gluon quasiparticles [12]. We note that there are no direct lattice measurements of quasiparticle dispersion curves below $1.5T_c$. One can infer quark quasiparticle masses from fits to thermodynamical observables and baryonic susceptibilities: it tells us that masses grow toward T_c , for a recent discussion see [13].

For further discussion it is convenient to introduce a dimensionless mass parameter $\tilde{m} = m/T$, which thus changes from large values close to T_c to about 3 at $1.5T_c$. Clearly, its value determines how accurate is the nonrelativistic approximation. For example, at $\tilde{m} = 5$ the mean square momentum $\sqrt{\langle p^2 \rangle}/T = 4.8$ if calculated relativistically, while the non-relativistic approximation gives the value smaller by a factor 0.8. The corresponding ratio of the total density in non-relativistic approximation is .7 of its relativistic value. So, it is not an unreasonable approximation, but not very accurate. At $T = 1.5T_c$ the

[§]In so far, our arguments were classical and nonrelativistic, so both \hbar and $1/c$ were set to zero. In this section, and this section only, we use the standard high energy units with $\hbar = 1, c = 1$. Hopefully, it will not create confusion for the reader. We will keep \hbar in the next formula, to emphasize the quantum origin of the repulsive core.

value of this mass is $\tilde{m} \approx 3$ only, and the accuracy of it is even worse. Therefore, we should calculate any momentum integrals relativistically, and only the results to be mapped into cQGP.

The color Casimir for gluons $C_g = 3$ and quarks $C_q = 4/3$ should be averaged over their respective weights. The number of effective degrees of freedom in thermodynamical quantities is such that roughly all three species – g, \bar{q}, q – are equally represented. Furthermore, the values of the coupling constant α_s inferred from measured static potentials at relevant distances is $\alpha_s \approx 0.5$. Withing the uncertainties, we will thus simply use $\langle \alpha_s C \rangle = 1$ below. Thus

$$\lambda = r_0 \approx \frac{1}{3T} \quad (38)$$

The density of quasiparticles n can be estimated as follows. Although quasiparticles are relatively heavy, the presence of bound states compensates and increases the density of total quasiparticles to about 0.8 of the entropy density per particle in the massless gas [14]. Ignoring this 0.8 which refers to the bound states, we then have

$$n \approx (0.244 T^3) (8 + 6 N_f) \approx 6.3 T^3 \quad (39)$$

where the first bracket is the usual density of black body radiation photons, and the second bracket is the number of effective degrees of freedom due to 8 colored gluons and 2 quarks and antiquarks with 3 colors and N_f flavors This corresponds to the following Wigner-Seitz radius

$$a_{WS} = \left(\frac{3}{4\pi n} \right)^{1/3} \approx \frac{1}{3T} \approx \lambda \quad (40)$$

The time units in MD are given by the plasma frequency, which is

$$\tau_0 = \omega_p^{-1} = \left(\frac{4\pi n \langle \alpha_s C \rangle}{m} \right)^{-1} \approx \frac{1}{5.1 T} \quad (41)$$

where, for definiteness, we used $m = 3T$.

In summary, the dimensionless cQGP results of the MD carried above can be qualitatively translated to the dimensionfull sQGP parameters using respectively the length λ , time τ_0 and mass m units

$$\begin{aligned} \lambda &\approx \frac{1}{3T} \\ \tau_0 &\approx \frac{1}{5.1 T} \\ m &\approx 3T \end{aligned} \quad (42)$$

with $\Gamma \approx 3$.

Indeed, the viscosity unit η_0 is then given by the combination of units with the appropriate dimension

$$\eta_0 = m/(\tau_0 \lambda) = (3T)(5.1T)(3T) \approx 46 T^3 \quad (43)$$

leading to the sQGP viscosity through

$$\eta \rightarrow \eta \eta_0 \approx (0.17)(46 T^3) \approx 7.8 T^3 \quad (44)$$

In the sQGP, it is customary to give the viscosity per entropy density, which for ideal massless QGP is

$$s_0 = \frac{4\pi^2}{90} \left(16 + \left(\frac{7}{8} \right) \times 2 \times 2 \times 3 \times N_f \right) T^3 \approx 20 T^3 \quad (45)$$

for 3 flavors. Correcting a bit for more realistic lattice entropy, we will use $s \approx 23 T^3$ around $T = 1.5 T_c$. Thus, the dimensionless viscosity $\eta \approx 0.17$ as measured in the one species cQGP above at $\Gamma \approx 3$, can be translated to the dimensionfull viscosity in the sQGP by rescaling through η_0 . The viscosity per entropy ratio in the sQGP is

$$\frac{\eta}{s} \rightarrow \frac{\eta \eta_0}{s} \approx 0.34 . \quad (46)$$

N=4 SYM results have suggested a universal lower bound for $\eta/s \geq 1/4\pi$. Our analysis suggests that in the sQGP this ratio is about 4 times the lower bound.

The diffusion constant translates to

$$D \approx 0.161 \rightarrow (0.161)(\lambda^2/\tau_0) \approx 0.1/T . \quad (47)$$

Similarly, the stress-tensor decorrelation time translates to

$$\tau_\eta \approx 0.395 \rightarrow (0.395)(\tau_0) \approx 0.08/T . \quad (48)$$

One should keep in mind, that these results are estimated for $T \approx 1.5 T_c$. As temperature gets closer to T_c , the masses of quasiparticles grow further and the coupling gets larger, so one finds even stronger coupled plasma. Unfortunately, we do not yet have sufficiently precise lattice data to make the mapping of the cQGP to the sQGP in this region more definite.

V. CONCLUSIONS AND PROSPECTS

Quarks and gluons in the temperature range of 1-1.5 T_c behave as quasiparticles with masses larger than $m > 3 T$ and a Casimir-weighted Coulomb strength of the order of $< C \alpha_s > \approx 1$ which is strong. Lattice measured potentials in this temperature range give $\Delta U/T$ between 20 at T_c and 5 at $1.2 T_c$ indicating the dominance of the potential energy over the thermal energy.

In this paper, we have suggested that the long-wavelength properties of the QGP in the 1-1.5 T_c range may be modeled by a classical and non-relativistic gas of massive quasi-particles interacting via strong but classical color charges. The model we coined cQGP has merits on its own and was analyzed numerically using molecular dynamics together with Wong's equations for classical color evolution.

Our results show the existence of several phases ranging from a gas-like phase at weak coupling, through

a liquid-like phase at intermediate coupling, and finally a crystal-like phase at strong coupling with anti-ferromagnetic-like color ordering. The transition from liquid to crystal is best seen in the density-density correlation function or its static counterpart the structure function. At large Coulomb coupling the excess energy per particle asymptotes the Madelung energy for a crystal.

We have used the numerical analysis to extract a number of transport coefficients including the quasiparticle diffusion constant, the bulk viscosity and relaxation time. While quantum mechanics is important in the sQGP in the formation of the underlying quasiparticles (dispersion laws) and the running of the coupling, we have suggested that the ensuing quasiparticle interaction and dynamics is essentially Coulombic and at strong coupling classical. For this, the cQGP results are generic at intermediate and strong coupling. We have given qualitative arguments for how to relate the cQGP transport results to those of interest in the sQGP by identifying the pertinent length scales. Indeed, we have found that the sQGP corresponds to $\Gamma \approx 3$ which is liquid-like and viscous with $\eta/s \approx 1/3 T$.

In a series of sequels to follow, we will provide more insights to the cQGP results presented above for the bulk, 2-particle correlations and transport properties.

Acknowledgments.

This work was partially supported by the US-DOE grants DE-FG02-88ER40388 and DE-FG03-97ER4014.

-
- [1] E. V. Shuryak, Phys. Lett. **B78** (1978) 150, Yadernaya Fizika **28** (1978) 796, Phys.Rep. **61** (1980) 71.
 - [2] E. Braaten and R. D. Pisarski, Nucl. Phys. B **337**, 569 (1990).
 - [3] D. Teaney, J. Lauret and E. V. Shuryak, Phys. Rev. Lett. **86**, 4783 (2001) [arXiv:nucl-th/0011058]. "A hydrodynamic description of heavy ion collisions at the SPS and RHIC," arXiv:nucl-th/0110037. P.F. Kolb, P.Huovinen, U. Heinz, H. Heiselberg, Phys. Lett. **B500** (2001) 232. Review in P. F. Kolb and U. Heinz, nucl-th/0305084.
 - [4] E. Shuryak, Prog. Part. Nucl. Phys. **53**, 273 (2004) [arXiv:hep-ph/0312227].
 - [5] E. V. Shuryak and I. Zahed, Phys. Rev. C **70**, 021901 (2004) [arXiv:hep-ph/0307267]. Phys. Rev. D **70**, 054507 (2004) [arXiv:hep-ph/0403127].
 - [6] M. Asakawa and T. Hatsuda, Nucl. Phys. **A715** (2003) 863c; S. Datta, F. Karsch, P. Petreczky and I. Wetzorke, Nucl. Phys. Proc. Suppl. **119**, 487 (2003) hep-lat/0208012.
 - [7] O. Kaczmarek, S. Ejiri, F. Karsch, E. Laermann and F. Zantow, hep-lat/0312015.

- [8] S.Ichimar, H.Iyetomi and S.Tanaka, Phys.Rep.149 (1986) 92-205
- [9] K. Johnson, Ann. Phys. (N.Y.) **192** (1989) 104.
- [10] S.K. Wong, Nuovo Cimento **A 65** (1970) 689.
- [11] J.P.Hansen and I.R.McDonald, Phys. Rev. **A11** (1975) 2111.
- [12] P. Petreczky, F. Karsch, E. Laermann, S. Stickan, I. Wetzorke, Nucl. Phys. Proc. Suppl. **106**, 513 (2002).
- [13] J. Liao and E. V. Shuryak, arXiv:hep-ph/0510110.
- [14] O. Kaczmarek, S. Ejiri, F. Karsch, E. Laermann and F. Zantow, **hep-lat/0312015**.